Supplementary Information

Structural and functional conservation of key domains in $InsP_3$ and ryanodine receptors

Min-Duk Seo[1*], Saroj Velamakanni[2*], Noboru Ishiyama[1], Peter B. Stathopulos[1], Ana M. Rossi[2], Samir A. Khan[2], Philippa Dale[2], Congmin Li[3], James B. Ames[3], Mitsuhiko Ikura[1] & Colin W. Taylor[2].

[1]Ontario Cancer Institute and Department of Medical Biophysics, University of Toronto, Ontario, M5G 1L7, Canada, [2]Department of Pharmacology, University of Cambridge, Tennis Court Road, Cambridge, CB2 1PD, UK, [3]Department of Chemistry, University of California, Davis, California, 95616, USA.

[*]These authors contributed equally.

Supplementary Discussion

Comparison of high-resolution structures of apo-NT/NT-$InsP_3$ and apo-$NT^{Cysless}$/$NT^{Cysless}$-$InsP_3$

A very recent report by Lin *et al.*[13], which appeared while our work was under review, presented 3.8 Å structures for the $InsP_3$-bound and apo states of wild-type NT derived from a single crystal grown in the presence of $InsP_3$. The backbone structures of these native forms are globally consistent with our separately derived apo- and $InsP_3$-bound structures of $NT^{Cysless}$ determined at 3.0 Å and 3.6 Å, respectively (Fig. 1-2). Lin *et al.* also identified static and dynamic interfaces between the SD:IBC-α and SD:IBC-β, respectively, in association with $InsP_3$-induced conformational changes[13]. However, a 3.0 and 3.8 Å comparison of the apo $2F_o$-F_c electron density maps (contoured at 1.5σ) allowed us to carry out a more precise determination of loop structures (e.g., residues 292-298) and side chain orientations within the α- and β-interfaces that are critical for allosteric regulation of the $InsP_3R$ (Supplementary Fig. 4). The published work[13] validates our use of $NT^{Cysless}$ to obtain higher atomic resolution data, which were critical for precisely defining interactions key to understanding the structural basis of $InsP_3R$ activation. Further, our more detailed apo-NT structure was used to locate the four NT subunits within the cryo-EM structure of a closed-$InsP_3R$ tetramer[10] by computational docking methods and to comprehensively interpret these data (Fig. 3 and Supplementary Fig. 6).

Interactions between the SD and TMD4-5

Considerable evidence suggests that the pores of $InsP_3R$ and RyR have a similar architecture to that of K^+ channels[6,21,22,39-44]. The last pair of TMDs (TMD 5-6 in RyR and $InsP_3R$) (Supplementary Fig. 1) from each of the four subunits are suggested to be arranged around a central pore, with TMD6 lining the pore and tapering towards its cytosolic side to form the narrowest part of the closed channel. The loop linking TMD5 to TMD6 are thought to form both a selectivity filter and a short pore helix that lie towards the luminal end of the channel. It is not yet clear whether these similarities in pore structure extend also to gating mechanisms.

In K^+ channels, a hinge part-way through the inner helix provides a pivot that allows the cytosolic end of each inner helix to splay outwards in the open channel[45,46]. A cryo-EM study of RyR1 reported a similar splaying of the inner helix (TMD6) in conditions expected to favour an open state[22]. However, in another structure, determined under similar conditions, the helix arrangement appeared more like a closed K^+ channel[44]. Furthermore, mutation of the conserved Gly residue that seemed most likely to form a hinge within TMD6 of either $InsP_3R1$ (G2586A)[42] or RyR2 (G4864A)[47] did not prevent $InsP_3R$ or RyR activation.

In voltage-gated K^+ channels, an amphipathic α-helix linking TMD4-5 that lies parallel to the cytosolic surface of the plasma membrane, links movement of the voltage-sensor in TMD4 to movement of the inner helix (TMD6)[48]. In other voltage-regulated channels too, the TMD4-5 loop is essential for gating[49]. The TMD4-5 loop of RyR and $InsP_3R$ is also predicted to form an amphipathic α-helix[50,51] and it is conserved between receptor subtypes, although it is longer in $InsP_3R$ than in RyR (Supplementary Fig. 11). Mutations within the TMD4-5 loop disrupt gating of $InsP_3R$[6,42] and RyR[50], a mimetic peptide activates RyR1[20], and the loop includes mutations of RyR that cause malignant hyperthermia[50]. From this and related evidence (main text), it has been suggested that the SD of one subunit may interact *directly* with the TMD4-5 loop of another[6]. It is not, however, the only mechanism proposed to link the SD to $InsP_3R$ gating[5].

Evidence supporting an interaction of the SD with the TMD4-5 loop includes the following. After digestion of $InsP_3R1$ with trypsin, fragments I (residues 1-345) and V (residues 1932-2749) remain

associated[51,52] and they can be covalently cross-linked[51]. The association of fragments I and V is disrupted by mutations in the TMD4-5 loop, which also increase $InsP_3$ binding and disrupt gating[6,8]. These results affirm the importance of the TMD4-5 loop, but the analyses were unable to eliminate a role for fragment III (residues 923-1581) in mediating interaction between N- and C-termini[51]. But the results also leave open the possibility that changes to the TMD4-5 loop allosterically affect regions elsewhere in fragment V (e.g., the C-terminal tail[5,8]) that might mediate interaction with the N-terminus. A recent study lends support to the latter suggestion by demonstrating that some mutations within the SD (Δ(67-108), E20A, D34K, S217A) that disrupt association of N- and C-termini do not affect $InsP_3$-evoked Ca^{2+} release[7,8]. Instead, the effects of mutations on the accessibility of the C-terminal tail are better correlated with their effects on $InsP_3R$ function[8]. Furthermore, the accessibility of this C-terminal region to trypsin cleavage[8], is regulated by Ca^{2+} and $InsP_3$. Collectively these data argue that the N and C-termini interact and that modifications to the TMD4-5 loop attenuate the interaction, but it remains unclear whether the interactions between the SD and TMD4-5 loop are direct.

In RyR, the TMD4-5 loop has been reported to interact with both the cytosolic C-terminal tail (residues 4938-5037)[53] and a region preceding the TMDs (95 kDa and including residues 4114-4142)[20]. Evidence that the interaction between the SD and TMD4-5 loop of $InsP_3R$ might be direct was provided by pull-down experiments in which isolated NT[51,54] or SD[7] associated with TMD regions that included the TMD4-5 loop[7,51,54]. NMR analysis of the interaction between the SD and peptides matching either half of the TMD4-5 loop have also suggested a direct interaction between them[7]. While these *in vitro* analyses are consistent with a direct interaction between the SD and TMD4-5 loop they cannot, of course, prove that the interactions occur in native tetrameric $InsP_3R$.

Evidence from docking our structure of the NT into a closed state of $InsP_3R1$ (Fig. 3a) suggests that the SD and TMD4-5 are too far apart for a direct interaction between them to be likely. We instead suggest, and in keeping with results from RyR[20,53], that both regions are essential for $InsP_3R$ activation, but the interaction between them is more likely to be indirect.

Supplementary References

39. Balshaw, D., Gao, L., and Meissner, G. Luminal loop of the ryanodine receptor: A pore-forming segment? *Proc. Natl. Acad. Sci. USA* **96**, 3345-3347 (1999).
40. Carney, J., Mason, S. A., Viero, C., and Williams, A. J. The ryanodine receptor pore: is there a consensus view? *Curr. Topics Membr.* **66**, 49-67 (2010).
41. Dellis, O., Dedos, S., Tovey, S. C., Rahman, T.-U.-., Dubel, S. J., and Taylor, C. W. Ca^{2+} entry through plasma membrane IP_3 receptors. *Science* **313**, 229-233 (2006).
42. Schug, Z. T., da Fonseca, P. C., Bhanumathy, C. D., Wagner, L., 2nd, Zhang, X., Bailey, B., Morris, E. P., Yule, D. I., and Joseph, S. K. Molecular characterization of the inositol 1,4,5-trisphosphate receptor pore-forming segment. *J. Biol. Chem.* **283**, 2939-2948 (2008).
43. Boehning, D. F. Molecular architecture of the inositol 1,4,5-trisphosphate receptor pore. *Curr. Topics Membr.* **66**, 191-207 (2010).
44. Ludtke, S. J., Serysheva, I. I., Hamilton, S. L., and Chiu, W. The pore structure of the closed RYR1 channel. *Structure* **13**, 1203-1211 (2005).
45. Jiang, Y., Lee, A., Chen, J., Cadene, M., Chait, B. T., and MacKinnon, R. The open pore conformation of potassium channels. *Nature* **417**, 523-526 (2002).
46. MacKinnon, R. Potassium channels and the atomic basis of selective ion conduction (Nobel Lecture). *Angew. Chem. Int. Edn. Engl.* **43**, 4265-4277 (2004).
47. Wang, R., Zhang, L., Bolstad, J., Diao, N., Brown, C., Ruest, L., Welch, W., Williams, A. J., and Chen, S. R. Residue Gln4863 within a predicted transmembrane sequence of the Ca^{2+} release channel (ryanodine receptor) is critical for ryanodine interaction. *J. Biol. Chem.* **278**, 51557-51565 (2003).
48. Long, S. B., Campbell, E. B., and MacKinnon, R. Voltage-sensor of Kv1.2: structural basis of electromechanical coupling. *Science* **309**, 903-908 (2005).
49. Voets, T., Owsianik, G., Janssens, A., Talavera, K., and Nilius, B. TRPM8 voltage sensor mutants reveal a mechanism for integrating thermal and chemical stimuli. *Nat. Chem. Biol.* **3**, 174-182 (2007).
50. Murayama, T., Kurebayashi, N., Oba, T., Oyamada, H., Oguchi, K., Sakurai, T., and Ogawa, Y. Role of amino-terminal half of the S4-S5 linker in the RyR1 channel gating. *J. Biol. Chem.* **286**, 35571-35577 (2011).

51. Boehning, D. and Joseph, S. K. Direct association of ligand-binding and pore domains in homo- and heterotetrameric inositol 1,4,5-trisphosphate receptors. *EMBO J.* **19**, 5450-5459 (2000).
52. Yoshikawa, F., Iwasaki, H., Michikawa, T., Furuichi, T., and Mikoshiba, K. Trypsinized cerebellar inositol 1,4,5-trisphosphate receptor. Structural and functional coupling of cleaved ligand binding and channel domains. *J. Biol. Chem.* **274**, 316-327 (1999).
53. Lee, E. H. and Allen, P. D. Homo-dimerization of RyR1 C-terminus via charged residues in random coils or in an alpha-helix. *Exp. Mol. Med.* **39**, 594-602 (2007).
54. Bultynck, G., Szlufcik, K., Kasri, N. N., Assefa, Z., Callewaert, G., Missiaen, L., Parys, J. B., and De Smedt, H. Thimerosal stimulates Ca^{2+} flux through inositol 1,4,5-trisphosphate receptor type 1, but not type 3, via modulation of an isoform-specific Ca^{2+}-dependent intramolecular interaction. *Biochem. J.* **381**, 87-96 (2004).
55. Joseph, S. K. Role of thiols in the structure and funciton of inositol trisphosphate receptors. *Curr. Topics Membr.* **66**, 299-322 (2010).
56. Sienaert, I., Kasri, N. N., Vanlingen, S., Parys, J., Callewaert, G., Missiaen, L., and De Smedt, H. Localization and function of a calmodulin/apocalmodulin binding domain in the N-terminal part of the type 1 inositol 1,4,5-trisphosphate receptor. *Biochem. J.* **365**, 269-277 (2002).
57. Nadif Kasri, N., Holmes, A. M., Bultynck, G., Parys, J. B., Bootman, M. D., Rietdorf, K., Missiaen, L., McDonald, F., De Smedt, H., Conway, S. J., Holmes, A. B., Berridge, M. J., and Roderick, H. L. Regulation of $InsP_3$ receptor activity by neuronal Ca^{2+}-binding proteins. *EMBO J.* **23**, 312-321 (2004).
58. Tu, J. C., Xiao, B., Yuan, J. P., Lanahan, A. A., Leoffert, K., Li, M., Linden, D. J., and Worley, P. F. Homer binds a novel proline-rich motif and links group 1 metabotropic glutamate receptors with IP_3 receptors. *Neuron* **21**, 717-726 (1998).
59. Ando, H., Mizutani, A., Kiefer, H., Tsuzurugi, D., Michikawa, T., and Mikoshiba, K. IRBIT suppresses IP_3 receptor activity by competing with IP_3 for the common binding site on the IP_3 receptor. *Mol. Cell* **22**, 795-806 (2006).
60. Patterson, R. L., van Rossum, D. B., Barrow, R. K., and Snyder, S. H. RACK1 binds to inositol 1,4,5-trisphosphate receptors and mediates Ca^{2+} release. *Proc. Natl. Acad. Sci. USA* **101**, 2328-2332 (2004).
61. Cui, J., Matkovich, S. J., deSouza, N., Li, S., Rosemblit, N., and Marks, A. R. Regulation of the type 1 inositol 1,4,5-trisphosphate receptor by phosphorylation at tyrosine 353. *J. Biol. Chem.* **279**, 16311-16316 (2004).
62. Malathi, K., Kohyama, S., Ho, M., Soghoian, D., Li, X., Silane, M., Berenstein, A., and Jayaraman, T. Inositol 1,4,5-trisphosphate receptor (type 1) phosphorylation and modulation by Cdc2. *J. Cell Biochem.* **90**, 1186-1196 (2003).
63. Bai, G. R., Yang, L. H., Huang, X. Y., and Sun, F. Z. Inositol 1,4,5-trisphosphate receptor type 1 phosphorylation and regulation by extracellular signal-regulated kinase. *Biochem Biophys Res Commun* **348**, 1319-1327 (2006).
64. Yang, L. H., Bai, G. R., Huang, X. Y., and Sun, F. Z. ERK binds, phosphorylates $InsP_3$ type 1 receptor and regulates intracellular calcium dynamics in DT40 cells. *Biochem. Biophys. Res. Commun.* **349**, 1339-1344 (2006).
65. Sienaert, I., Missiaen, L., De Smedt, H., Parys, J. B., Sipma, H., and Casteels, R. Molecular and functional evidence for multiple Ca^{2+}-binding domains on the type 1 inositol 1,4,5-trisphosphate receptor *J. Biol. Chem.* **272**, 25899-25906 (1997).
66. Dal Santo, P., Logan, M. A., Chisholm, A. D., and Jorgensen, E. M. The inositol trisphosphate receptor regulates a 50-second behavioral rhythm in *C. elegans*. *Cell* **98**, 757-767 (1999).
67. Joseph, S. K., Brownell, S., and Khan, M. T. Calcium regulation of inositol 1,4,5-trisphosphate receptors. *Cell Calcium* **38**, 539-546 (2005).
68. Meur, G., Parker, A. K. T., Gergely, F. V., and Taylor, C. W. Targeting and retention of type 1 ryanodine receptors to the endoplasmic reticulum. *J. Biol. Chem.* **282**, 23096-23103 (2007).
69. Laude, A. J., Tovey, S. C., Dedos, S., Potter, B. V. L., Lummis, S. C. R., and Taylor, C. W. Rapid functional assays of recombinant IP_3 receptors. *Cell Calcium* **38**, 45-51 (2005).
70. Berridge, M. J., Bootman, M. D., and Roderick, H. L. Calcium signalling: dynamics, homeostasis and remodelling. *Nat. Rev. Mol. Cell Biol.* **4**, 517-529 (2003).
71. Guse, A. H. Cyclic ADP-ribose. *J. Mol. Med.* **78**, 26-35 (2000).
72. Churamani, D., Boulware, M. J., Geach, T. J., Martin, A. C., Moy, G. W., Su, Y. H., Vacquier, V. D., Marchant, J. S., Dale, L., and Patel, S. Molecular characterization of a novel intracellular ADP-ribosyl cyclase. PLoS One **2**, e797 (2007).

Supplementary Table 1 | Sequences of N-terminal fragments and chimeric proteins

IBC	$InsP_3R1$ (224-604)
NT	$InsP_3R1$ (1-604)
$NT^{Cysless}$	$InsP_3R1$ (1-604), all Cys replaced by Ala
RyR2A-IBC	RyR2 (1-210) – $InsP_3R1$ (225-604)
RyR1A-$InsP_3R1$	RyR1 (1-210) – $InsP_3R1$ (225-2748)
$InsP_3R1$-RyR1	$InsP_3R1$ (1-2274) – RyR1 (4511-5037)

Supplementary Figure 11 compares the sequences of the chimeric proteins.

Supplementary Table 2 | $InsP_3$ binding to Cys-less and native N-terminal fragments of $InsP_3R1$

	K_D (nM)	**pK_D**	**Hill coefficient**
IBC	0.14	9.85 ± 0.21	1.15 ± 0.04
$IBC^{Cysless}$	0.15	9.83 ± 0.21	1.21 ± 0.09
NT	2.82	8.55 ± 0.18	1.06 ± 0.20
$NT^{Cysless}$	2.75	8.56 ± 0.15	1.03 ± 0.18

Results (means ± s.e.m., $n \geq 3$; mean only for K_D) show the affinity (K_D and pK_D) and Hill coefficient for $InsP_3$ binding to the indicated N-terminal fragments of $InsP_3R1$.

Supplementary Table 3 | Data collection and refinement statistics for $NT^{Cysless}$

	Apo-$NT^{Cysless}$	$InsP_3$-bound $NT^{Cysless}$
Data collection		
Space group	P1	C121
Cell dimensions		
a, b, c (Å)	63.1, 77.2, 101.5	189.2, 78.7, 134.1
α, β, γ (°)	105.4, 100.0, 101.0	90.0, 124.5, 90.0
Wavelength (Å)	0.97924	0.97915
Resolution range (Å)	50-3.0 (3.05-3.0)	50-3.6 (3.66-3.6)
R_{sym}(I) (%)	7.3 (32.9)	8.0 (45.2)
I/σ(I)	21.3 (3.9)	13.5 (2.2)
Number of reflections	33022	18075
Completeness (%)	98.6 (98.5)	99.8 (100.0)
Redundancy	3.8 (3.7)	3.7 (3.8)
Z value	2	4
Refinement		
R_{cyst}/R_{free} (%)	20.8/25.6	25.8/30.8
No. atoms*		
Protein	7421	7722
Ligand/ion	5	48
Water	28	9
B-factors ($Å^2$)		
Protein	40.0	70.05
Ligand/ion	72.6	153.1
Water	50.0	89.4
Ramanchandram statistics		
Most favorable regions (%)	93.3	87.3
Allowed regions (%)	6.7	12.7
Disallowed regions (%)	0.0	0.0
R.m.s deviations		
Bond lengths (Å)	0.0067	0.0062
Bond angles (°)	1.1250	1.1155

Values in parentheses are for the highest resolution shell.
*The numbers of atoms are for the two molecules in the asymmetric unit.

Supplementary Table 4 | $InsP_3$ binding to mutant NT

	K_D (nM)	pK_D	Hill coefficient
IBC	0.15	9.84 ± 0.19	0.97 ± 0.11
NT	2.21	8.66 ± 0.07	1.04 ± 0.07
NT^{V33K}	0.26	9.58 ± 0.05	1.03 ± 0.12
NT^{D34K}	0.66	9.18 ± 0.03	1.11 ± 0.06
NT^{R36E}	0.39	9.41 ± 0.14	1.11 ± 0.04
NT^{K52E}	2.56	8.59 ± 0.05	0.93 ± 0.03
NT^{K127E}	0.43	9.36 ± 0.07	1.03 ± 0.08

Results (means ± s.e.m., n = 4-10; mean only for K_D) show the affinity (K_D and pK_D) and Hill coefficient for $InsP_3$ binding to N-terminal fragments. These measurements, in contrast to those shown in Supplementary Tables 2 and 6, are from analyses of bacterial lysates (not purified protein) after treatment with thrombin to cleave an N-terminal His_6-tag[4]. There is no significant difference in the binding properties of the NT and IBC determined using the two assays.

Supplementary Table 5 | Distribution of key functional sites within the NT of $InsP_3R1$

	Residues	Ref.
Trypsin cleavage	R345	52
Accessible Cys: native or (SCAM)	C206, C214 (C326 in SI site), C553[a] (S2C, S6C, S7C, A189C, S277C)	15, 55
Inaccessible Cys (SCAM)	(S217C, A245C, S436C)	15
Accessible Cys after Ca^{2+} (SCAM)	(S171C, S277C, A575C)	15
Calmodulin	P49-N81 and E106-S128	56
CaBP1	P49-N81	57
Homer	N48-D55	58
IRBIT	Probably overlaps $InsP_3$-binding site	59
RACK1	N90-L110 and F580-H600	60
Phosphorylation (fyn)	Y353	61
Phosphorylation (cdc2)	S421	62
Phosphorylation (ERK)	S436	63, 64
Ca^{2+}-binding sites[b]	R304-L381 and G378-S450	65
Possible Ca^{2+}-binding sites (Ca-I and Ca-II)[c]	Ca I: E246, E425, D426 and E428 CaII: E283, E285, D444 and D448	2
Null allele in *C elegans*	G25E	66

CaBP1, Ca^{2+}-binding protein 1; IRBIT, $InsP_3$ receptor-binding protein released with $InsP_3$; RACK1, receptor for activated C-kinase 1; SCAM, scanning cysteine accessibility mutagenesis.
[a]By analogy with reactive Cys conserved in RyR[55].
[b]Ca^{2+} binding to these peptide was demonstrated by $^{45}Ca^{2+}$ overlay, but point mutations of conserved acidic residues within the second site (E411Q, D426N, E428Q, E439Q, D442N and D444N) had no effect on Ca^{2+} stimulation of $InsP_3$-evoked Ca^{2+} release by $InsP_3R$[67].
[c]It has been suggested that these clusters of acidic residues, first identified in the structure of the IBC[2], may form Ca^{2+}-binding sites. Some of the residues (E428Q, D444N) have been mutated without affecting Ca^{2+} stimulation of $InsP_3R$ gating[67].

The locations of these key sites within the NT docked into the closed state of $InsP_3R1$ are shown in Supplementary Figure 6c.

Supplementary Table 6 | $InsP_3$ binding to RyR2A-IBC and its mutants

	K_D (nM)	pK_D	Hill coefficient
IBC	0.27	9.56 ± 0.09	0.84 ± 0.08
NT	2.0	8.70 ± 0.04	1.0 ± 0.1
RyR2A-IBC	1.84	8.73 ± 0.04	1.4 ± 0.15
$RyR2A^{E40K}$-IBC	0.98	9.01 ± 0.08	1.0 ± 0.05
$RyR2A^{G41K}$-IBC	0.42	9.37 ± 0.15	0.7 ± 0.1
$RyR2A^{G43K}$-IBC	2.26	8.65 ± 0.04	1.2 ± 0.16

Results (means ± s.e.m., n = 4; mean only for K_D) show the affinity (K_D and pK_D) and Hill coefficient for $InsP_3$ binding to the indicated chimeric N-terminal fragments.

Supplementary Table 7 | $InsP_3$-evoked Ca^{2+} release by $InsP_3R1$ and its chimeras stably expressed in DT40 cells

	EC_{50} (nM)	pEC_{50}	Maximal Ca^{2+} release (%)	Expression (%)
$InsP_3R1$	56	7.25 ± 0.05	58 ± 2	100
RyR1A-$InsP_3R1$	110	6.96 ± 0.22	64 ± 7	101 ± 23
$InsP_3R1$-RyR1	1202	5.92 ± 0.08	57 ± 5	106 ± 17

Results (means ± s.e.m., n = 3; mean only for EC_{50}) show the effects of $InsP_3$ on Ca^{2+} release from DT40 cells stably expressing the indicated $InsP_3R$. Expression levels of each $InsP_3R$ (relative to paired comparisons with $InsP_3R1$) were determined from Western blots similar to those shown in Supplementary Figure 9a and b.

Supplementary Table 8 | Primers used to generate NT^{Cysless} (mutated residues are underlined)

Residue	Primer sequence (5'-3')
15	CATATCGGAGACATT**GCT**TCTCTGTATGCAGAG
37	TTGGTTGATGACCGT**GCC**GTTGTACAGCCAGAA
56 & 61	TTCAGAGAC**GCC**CTCTTTAAGCTA**GCT**CCTATGAAT
206 & 214	CCGGGC**GCC**AATGAGGTCAACTCCGTCAAC**GCT**AACACA
253	GAGAAGTTTCTCACG**GCC**GATGAGCACAGGAAG
292	GTCCAGCATGACCCA**GCT**CGGGGTGGAGCTGGG
394	CGGCTCAGACACCTG**GCT**ACAAACACCTGGGTT
530	TTCACGGAC**GCC**GGGGATGGCCCAATGCTT
553 & 556	GCTCCTTTCAGACACATT**GCC**CGACTC**GCC**TACAGGGTCCTGAGA

Supplementary Table 9 | Primers used to generate mutant forms of RyR2A-IBC and NT (F, forward; R, reverse; mutated residues are underlined)

Construct		Primer sequence (5'-3')
RyR2A^{E40K}-IBC	F	AGCTATGCTTGGCAGC**AAA**AGGATTTGGCAACAGA
	R	TCTGTTGCCAAATCC**TTT**TGCTGCCAAGCATAGCT
RyR2A^{G41K}-IBC	F	GAAACAAAGTCTGTTGCCAAA**TTT**TTCTGCTGCCAAGCATAGCTTC
	R	GAAACAAAGTCTGTTGCCAAA**TTT**TTCTGCTGCCAAGCATAGCTTC
RyR2A^{G43K}-IBC	F	AGCTATGCTTGGCAGCAGAAGGATTT**AAG**AACAGACTTTGTTTCTTGG
	R	CCAAGAAACAAAGTCTGTT**CTT**AAATCCTTCTGCTGCCAAGCATAGCT

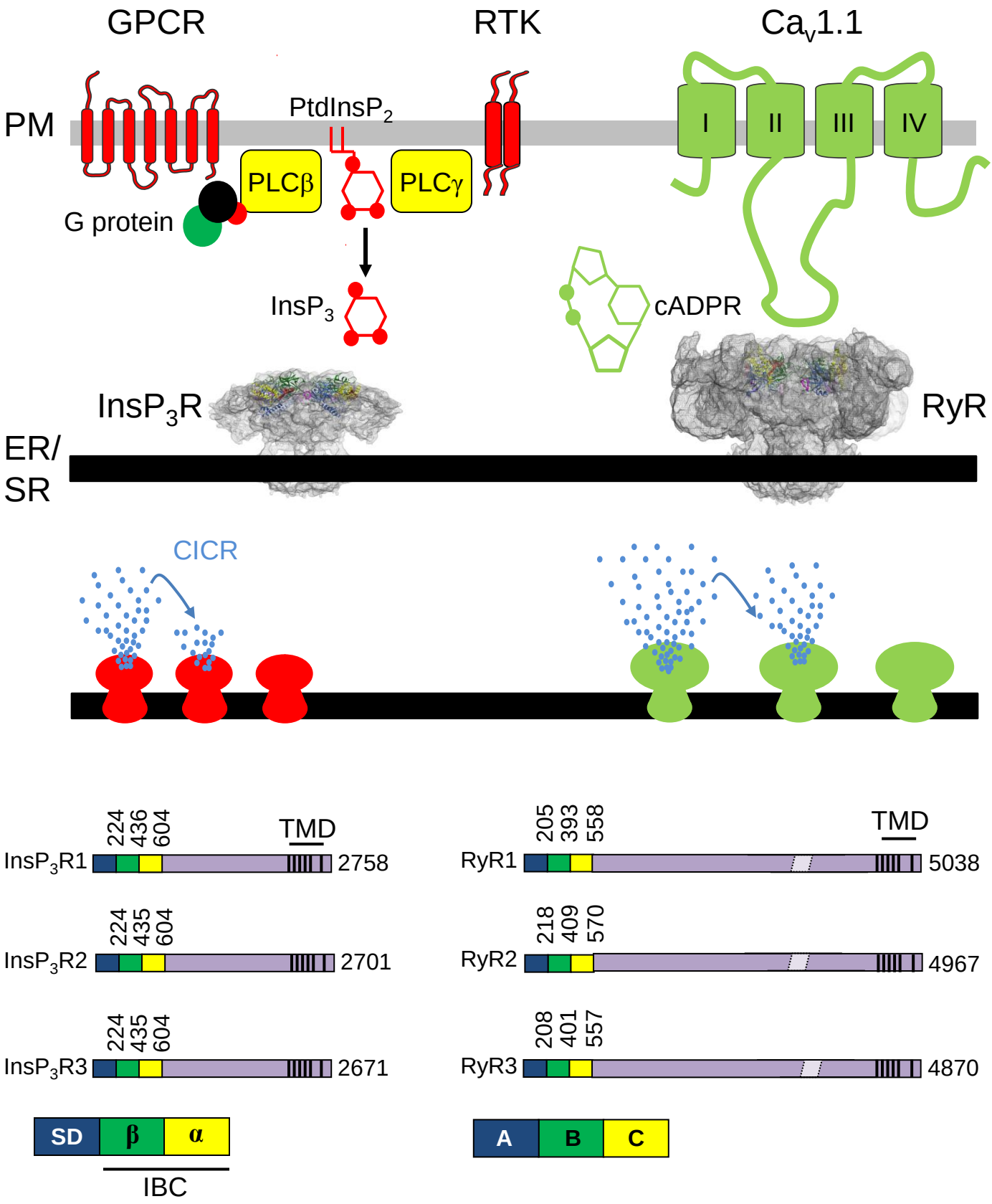

Supplementary Figure 1 | $InsP_3R$ and RyR allow extracellular stimuli to release Ca^{2+} from intracellular stores. Legend on next page.

Supplementary Figure 1 | $InsP_3R$ and RyR allow extracellular stimuli to release Ca^{2+} from intracellular stores. $InsP_3R$ are almost ubiquitously expressed in animal cells and RyR are widely expressed, but most prominently in skeletal muscle (RyR1) and cardiac muscle (RyR2)[1]. Many cells co-express RyR and $InsP_3R$. Both families of receptors form intracellular Ca^{2+} channels that are expressed predominantly in the membranes of the endoplasmic reticulum (ER) or sarcoplasmic reticulum (SR) in muscle[14]. They release Ca^{2+} from the ER/SR to the cytosol when appropriate stimuli cause the pores of the channels to open. IP_3R and RyR are therefore essential links between diverse extracellular stimuli and the release of Ca^{2+} from intracellular stores[70].

Extracellular stimuli (hormones, neurotransmitters or growth factors) are recognized by receptors in the plasma membrane (PM) that lead to activation of phospholipase C (PLC). PLC catalyses hydrolysis of the membrane lipid, phosphatidylinositol 4,5-bisphosphate ($PtdInsP_2$) to produce diacylglycerol and $InsP_3$. Stimuli that are recognized by G protein-coupled receptors (GPCR) cause activation of PLCβ isoforms via G proteins, while activation of receptors with intrinsic tyrosine kinase activity (RTK) causes recruitment and activation of PLCγ. The cytosolic messenger, $InsP_3$, links activation of these receptors in the PM to gating of $InsP_3R$ in the ER and thereby to cytosolic Ca^{2+} signals[70]. Another cytosolic messenger, cyclic ADP ribose (cADPR), which is synthesized from β-nicotinamide adenine dinucleotide (NAD^+) by enzymes that remain poorly understood[71,72], can activate RyR. In addition, depolarization of the PM in skeletal muscle activates RyR1 in the SR by conformational coupling to an intracellular loop of a voltage-sensing Ca^{2+} channel in the PM ($Ca_v1.1$)[1]. Both $InsP_3R$ and RyR are also biphasically regulated by cytosolic Ca^{2+}, with important physiological consequences. Inhibition by high cytosolic [Ca^{2+}] may contribute to feedback inhibition of channel activity, while stimulation by lesser increases in cytosolic [Ca^{2+}] allows the channels to mediate Ca^{2+}-induced Ca^{2+} release (CICR). CICR allows IP_3R and RyR both to respond to Ca^{2+} entering the cytosol via other Ca^{2+} channels and to mediate regenerative Ca^{2+} signals. The latter are important in defining the spatial organization of cytosolic Ca^{2+} signals and thereby the final cellular response.

Vertebrates have genes that encode three closely related $InsP_3R$ subunits ($InsP_3R1$-3) each of about 2700 residues, and three closely related RyR subunits of about 5000 residues (RyR1-3). Functional $InsP_3R$ and RyR are tetrameric assemblies of these subunits. While $InsP_3R$ form both homo- and hetero-tetramers, RyR probably form only homo-tetramers. There are probably six transmembrane domains (TMD1-6) towards the C-terminal of each subunit, and the pore is formed by a tetrameric association of the TMD5-6 regions (Supplementary Fig. 11). The linear representations of the primary sequences of $InsP_3R1$-3 and RyR1-3 (numbering refers to human sequences) highlight the three N-terminal regions of each and the location of the transmembrane domains (TMD), the last pair of which form the pore.

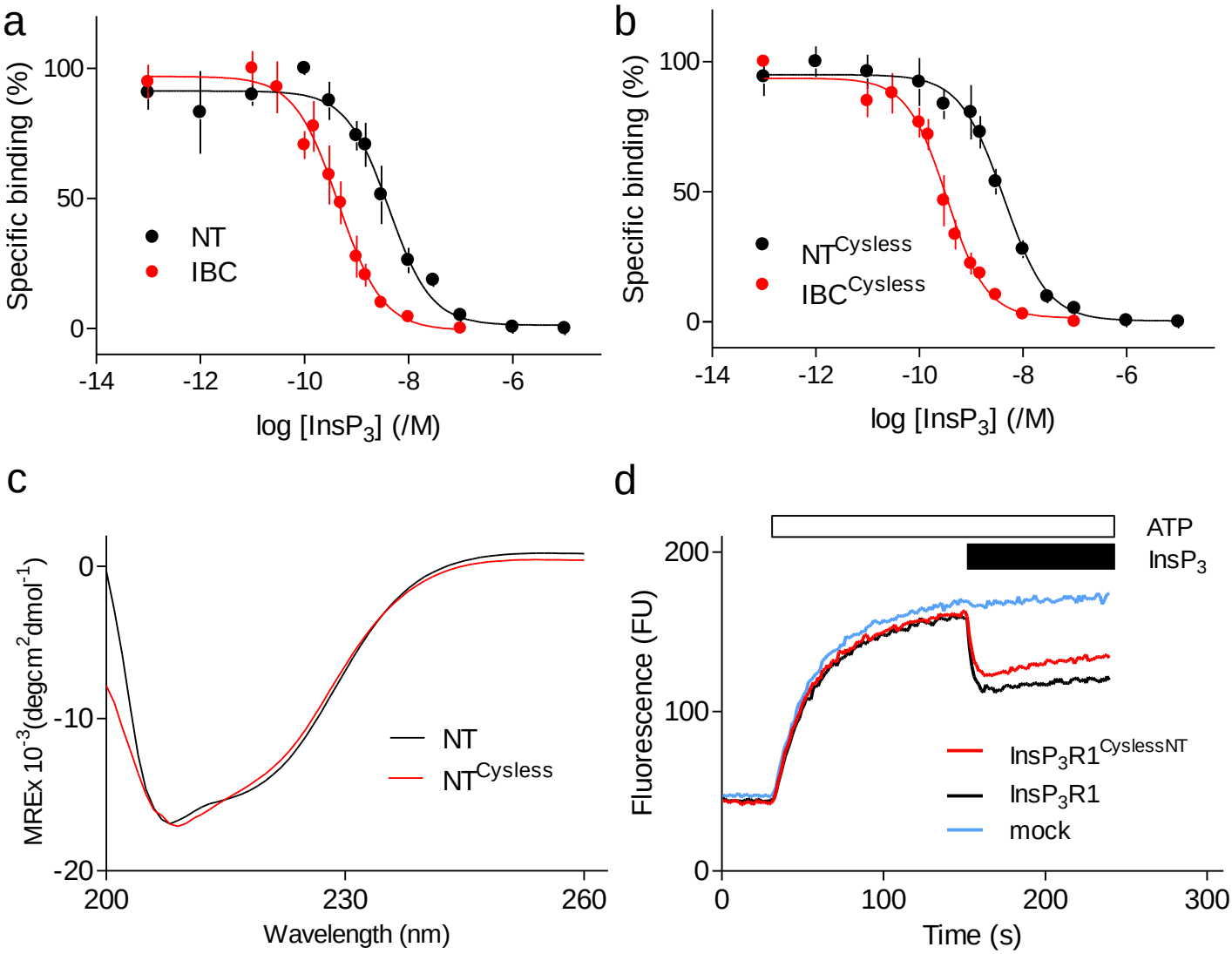

Supplementary Figure 2 | Properties of native and Cys-less NT of $InsP_3R1$. a, **b**, Specific binding of ^3H-$InsP_3$ to the IBC and NT of wild-type (**a**) and Cys-less (**b**) proteins shows that replacement of all Cys with Ala has no effect on $InsP_3$ binding. Results (**a**, **b**) are means ± standard error of the mean (s.e.m.), n = 3. Supplementary Table 2 summarizes the $InsP_3$-binding properties of these fragments. **c,** Far-UV CD spectra of wild-type NT (black) and $NT^{Cysless}$ (red) in the absence of $InsP_3$. **d**, We have not been able to establish DT40 cell lines stably expressing $InsP_3R1$ with a Cys-less N-terminal ($InsP_3R1^{CyslessNT}$), we therefore assessed $InsP_3$-evoked Ca^{2+} release using permeabilized DT40 cells after transient transfection with plasmids encoding $InsP_3R$. Typical results show Ca^{2+} uptake into the intracellular stores after addition of ATP, and $InsP_3$-evoked Ca^{2+} release from cells transiently expressing $InsP_3R1$ or $InsP_3R1^{CyslessNT}$. The parental cells (DT40-KO, mock transfected), which lack $InsP_3R$, do not respond to $InsP_3$. In parallel experiments with EGFP-$InsP_3R1$, the transfection efficiency was 36 ± 3% (mean ± s.e.m., n = 4). The lesser $InsP_3$-evoked Ca^{2+} release (~25-30%) from these populations of transiently transfected cells is consistent with the transfection efficiency and Ca^{2+} release observed from stably transfected cells (60-70% Ca^{2+} release, Supplementary Table 7). We conclude that $InsP_3R$ and $InsP_3R1^{CyslessNT}$ similarly mediate $InsP_3$-evoked Ca^{2+} release.

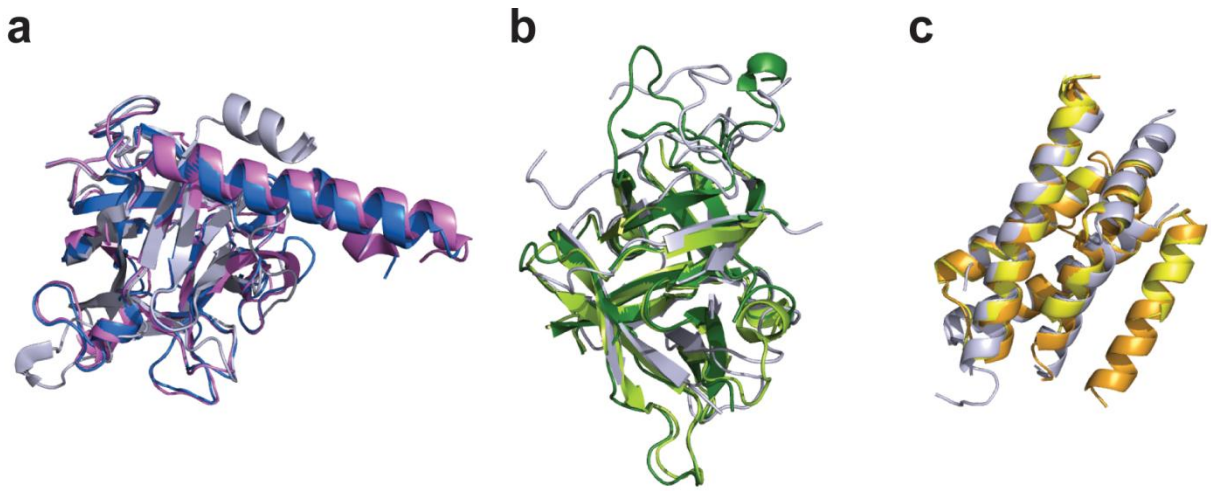

Supplementary Figure 3 | Structural similarities of the three N-terminal domains of $InsP_3R1$ and RyR1. a, Superposition of the isolated structures of the wild-type SD (purple), $SD^{Cysless}$ (blue) and RyR1-A (grey). **b**, **c**, The IBC-β domain (**b**, green) and IBC-α domain (**c**, yellow) of apo-$IBC^{Cysless}$ were separately superposed with the equivalent domains of $InsP_3$-bound IBC[2] (PDB code 1N4K) (light green and orange, respectively) and with the B and C domains of RyR1[9] (PDB code, 2XOA) (grey). The three NT domains of IP_3R1 (SD, IBC-β and IBC-α) individually superpose to the corresponding domains of RyR1 (A, B and C) with backbone root mean square deviations (r.m.s.) of 1.6 Å, 1.9 Å and 1.3 Å, respectively. Colour-coding of the domains matches that used in Figure 1.

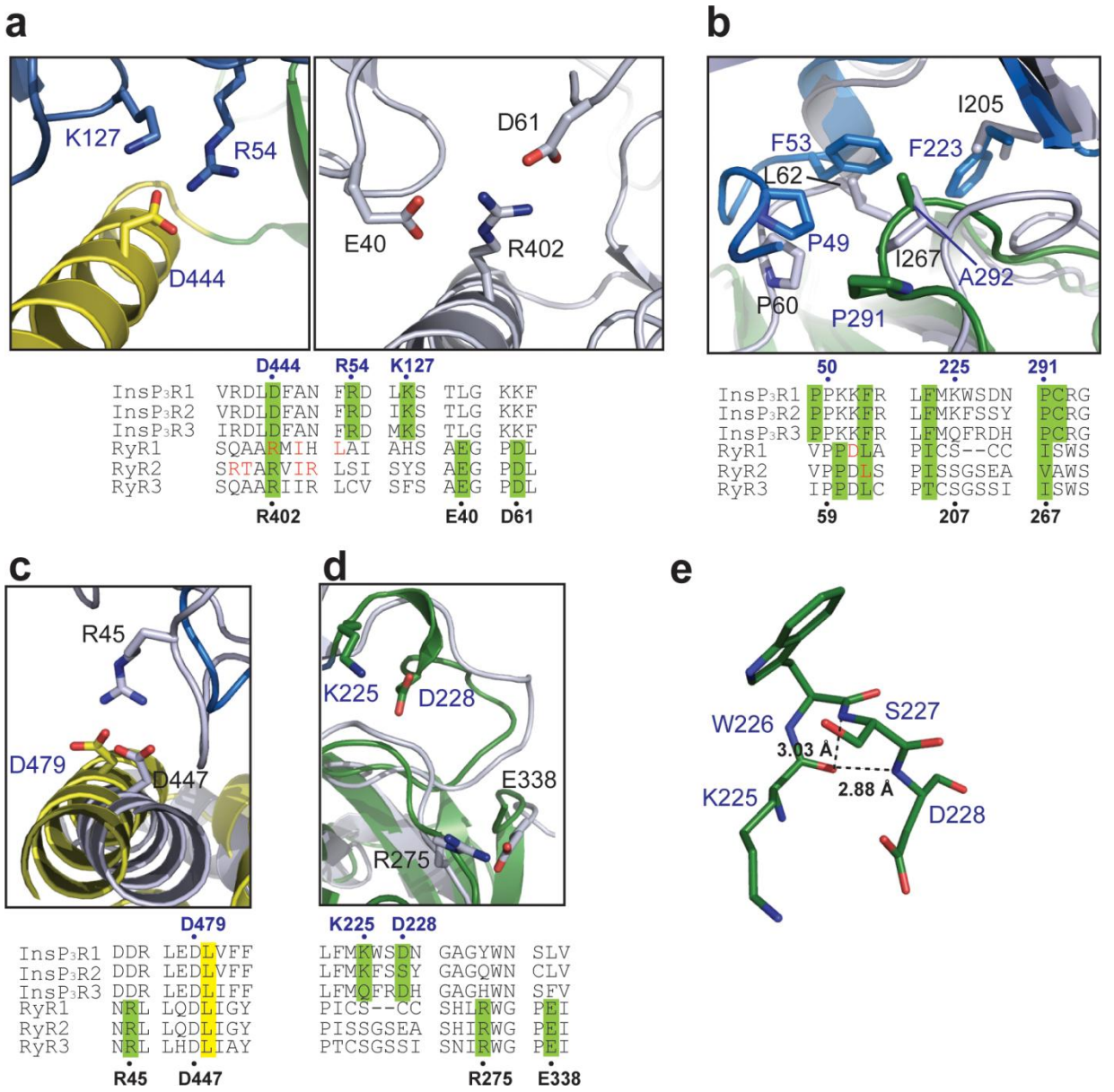

Supplementary Figure 4 | Comparison of the α- and β-interfaces of InsP$_3$R1 and RyR1. a, Critical salt bridges at the α-interface in InsP$_3$R (left) and A-C interface in RyR1 (right) are shown. **b**, Superposition of hydrophobic core residues at the β-interface (InsP$_3$R1, blue and green; blue lettering) and A-B interface (RyR1, grey; black lettering). Residues involved in salt bridge formation or hydrophobic interactions are shaded green in the structure-based sequence alignments. **c**, Superposed structures of the SD/IBC-α interface of InsP$_3$R1 (blue and yellow) with the RyR1 A-C interface (grey) show that a salt bridge in RyR1 is formed between R45 and D447; the conserved charged residue in InsP$_3$R1 (D479) is exposed but it does not form a salt bridge. **d**, Residues that form electrostatic interactions at the SD/IBC-β interface: K225-D228 in InsP$_3$R1(green), and R275 and E338 in the RyR1 A-B interface (grey) differ between the two receptors. The domain interface residues are shaded green in the structure-based sequence alignments. Blue and black labelling refer to InsP$_3$R1 and RyR1, respectively. **e**, Close-up view of the 3^{10}-like turn between the SD and IBC-β of apo-InsP$_3$R. The carbonyl group of K225 is predicted to hydrogen bond with the amide groups of S227 and D228. The hydrogen bond distances are shown with broken lines.

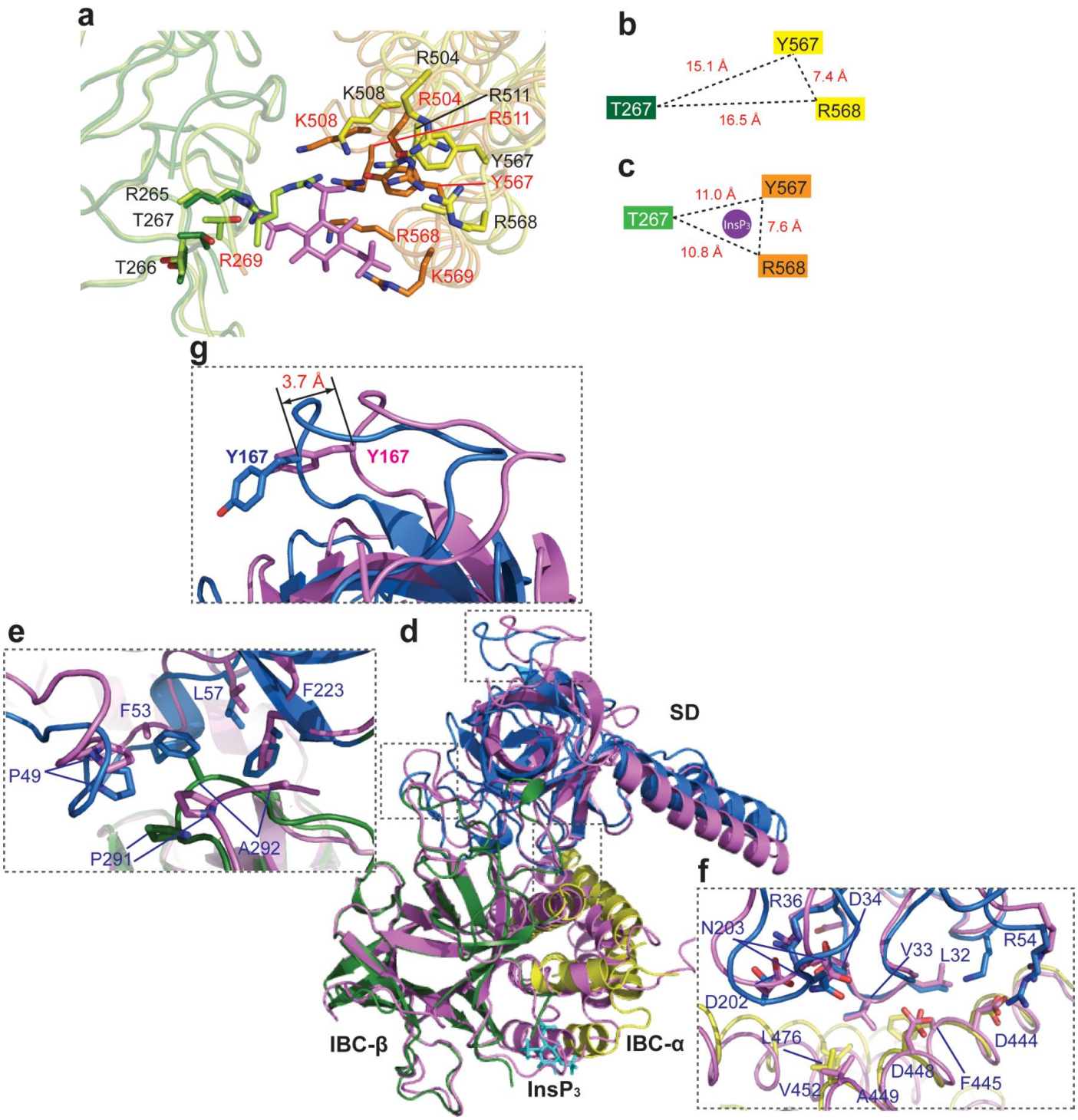

Supplementary Figure 5 | $InsP_3$ binding causes partial closure of the clam-like IBC and twisting of the SD. a, $InsP_3$-coordinating residues are shown as sticks in the apo- (black labels) and $InsP_3$-bound (red labels) states by superposing the IBC-β domains of the apo-$NT^{Cysless}$ structure (IBC-α, yellow; IBC-β, dark green) and the IBC-$InsP_3$ structure in isolation (orange and green; PDB code: 1N4K)[2]. **b**, **c**, Schematic representations of the apo- and $InsP_3$-bound $InsP_3$-binding cleft with distances between key $InsP_3$-coordinating residues indicated. **d**, Superposition of the apo-$NT^{Cysless}$ (SD, blue; IBC-α, yellow; IBC-β, green) and the $InsP_3$-bound $NT^{Cysless}$ (3.6 Å resolution, magenta) by overlaying the IBC-β domains. The view is rotated 45° about the y axis relative to Fig. 2. The β-interface (**e**), α-interface (**f**), and conserved HS-loop (**g**) are highlighted (dashed rectangles). **e**, **f**, Comparison of the β-interface (**e**) and α-interface (**f**) in the apo- and $InsP_3$-bound structures. Residues that form hydrophobic/electrostatic interactions in each structure are represented by sticks. **g**, Close-up views of the conserved HS-loop region, with the side chains of Y167 depicted by sticks. The distance between α-carbons of Y167 in the two states is marked (~3.7 Å).

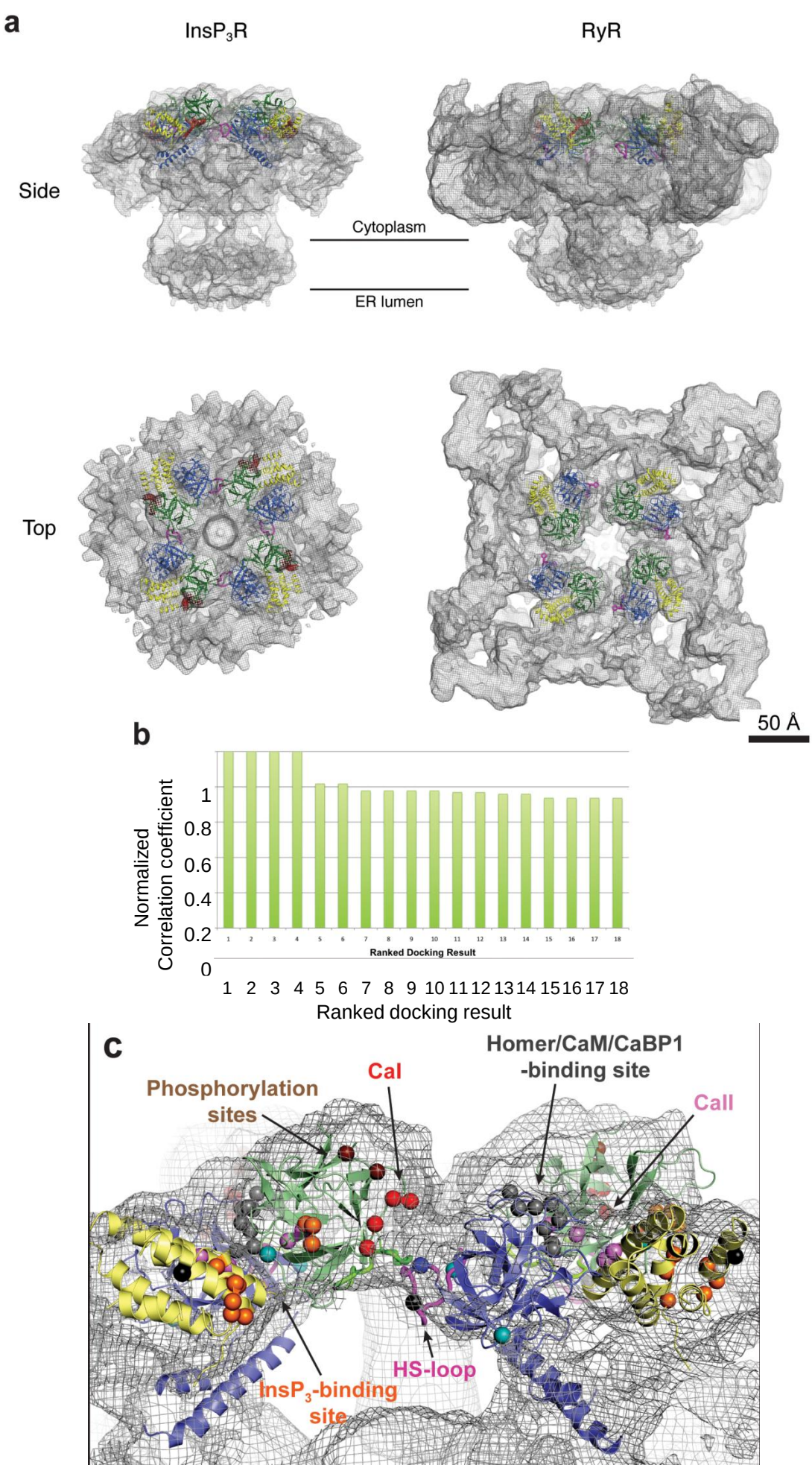

Supplementary Figure 6 | Comparison of the arrangement of the N-terminal structures of $InsP_3R1$ and RyR1 docked into the cryo-EM maps of the complete receptors. Legend on next page.

Supplementary Figure 6 | Comparison of the arrangement of the N-terminal structures of $InsP_3R1$ and RyR1 docked into the cryo-EM maps of the complete receptors. a, Side and top views of the apo-$NT^{Cysless}$ structures fitted into the cryo-EM structure of $InsP_3R1$[10] and of the RyR1-ABC structures fitted into the cryo-EM structure of RyR1[9]. The cryo-EM maps of $InsP_3R1$ tetramer (1.3 MDa) and RyR1 tetramer (2.2 MDa) contoured at protein density of 0.8 and 0.7 Da/$Å^3$, respectively, are shown. For both $InsP_3R1$ and RyR1, rigid-body docking using Laplacian filtering (see Methods) resulted in top solutions placing four molecules around the four-fold symmetry axis in the cytoplasmic portion of each receptor. As previously reported[9], searching the RyR1-A and RyR1-BC fragments independently in the cryo-EM structure of RyR1 located these domains in the same places found by the search using the RyR-ABC. In contrast, docking of the SD and IBC domains independently into the $InsP_3R1$ structure was unsuccessful, as previously reported[10]. Equivalent domains of $InsP_3R$ and RyR are shown in the same colours: SD and RyR-A (blue), IBC-β and RyR-B (green), and IBC-α and RyR-C (yellow). In $InsP_3R1$, the C-terminal of IBC-α surrounds a closed ring formed by four pairs of the SD and IBC-β domains. Similarly in RyR1, RyR1-C surrounds a ring formed by four RyR-AB pairs. The $InsP_3$-binding sites (red) are ~80 Å apart and face away from the centre of the ring. The HS-loop of the SD and the 'hot-spot' loop of RyR1-A are highlighted in magenta (see Fig. 3c,d). The apo-$NT^{Cysless}$ and RyR1-ABC structures viewed from the top are shown superposed in Figure 3b-d. **b,** Normalized correlation coefficients for the top 18 hits after docking the apo-$NT^{Cysless}$ structure into the cryo-EM structure of $InsP_3R1$[10] using SITUS[38]. There are four equally ranked top hits with a high docking contrast[9], reflecting the four subunits in the homotetrameric assembly of $InsP_3R1$. C, **c**, Close-up view of two docked apo-$NT^{Cysless}$ (dashed box in view alongside). The HS-loop of the SD is near a loop (β20-β21) in IBC-β (green) of the adjacent NT. The panel shows locations of putative Ca^{2+}-bindings sites (CaI and CaII)[2]; Y167 (blue), which is required for $InsP_3R$ activation[8]; phosphorylation sites (brown); proposed binding sites for Homer, calmodulin (CaM) and CaBP1 (grey); and key residues within the HS-loop that are accessible (blue), or accessible only after addition of Ca^{2+} (black). The $InsP_3$-binding sites (orange) are exposed and ~80 Å apart. Further details of the binding sites within the NT are provided in Supplementary Table 5.

Supplementary Figure 7 | Structure-based sequence alignment of the N-terminal region of $InsP_3R$ and RyR. DALI server (DALILite) was used to produce structure-based sequence alignments of the three subtypes of rat $InsP_3R$ and rabbit RyR. Residues conserved in all six sequences are highlighted by pink shading. $InsP_3$-coordinating residues are shaded red, residues associated with disease in RyR1 and RyR2 are coloured red, and the HS-loop regions are boxed red. Secondary structure elements of $InsP_3R$ are represented by arrows (β-strands) and bars (α-helices). Missing regions are shown as dotted lines. The colours of the SD (blue), IBC-β (green) and IBC-α (yellow) are consistent with Figure 1.

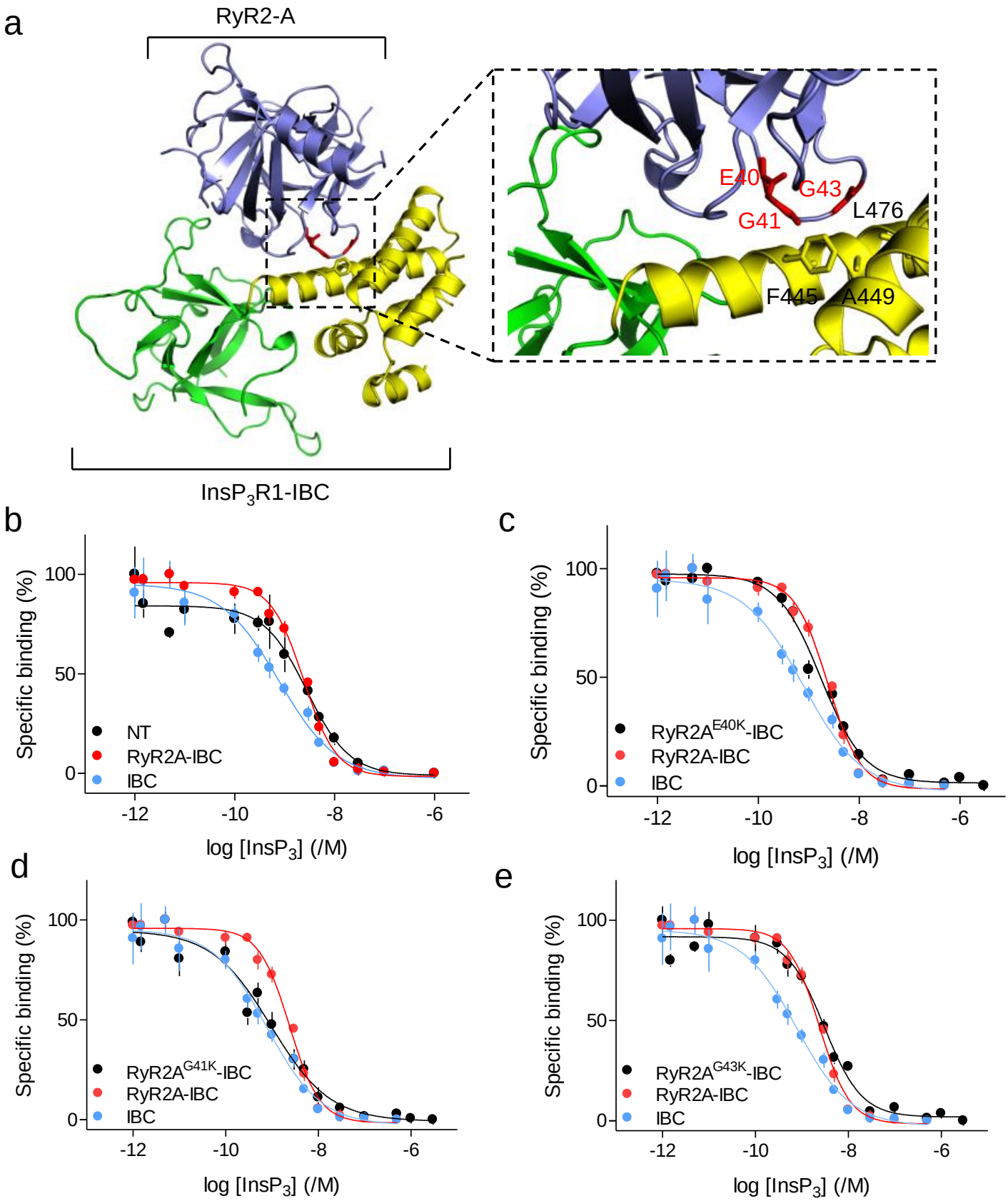

Supplementary Figure 8 | The A-domain of RyR2 mimics the effects of the SD on $InsP_3$ binding to the IBC. a, A model structure of the RyR2A-IBC chimera produced by superposing the structure of the A domain of RyR2 (PDB: 3IM5)[12] onto the SD of the $NT^{Cysless}$ (see Methods for details). Key residues (E40, G41 and G43) within the A domain that contribute to the α-interface are highlighted in red. **b**, Specific binding of ^{3}H-$InsP_3$ to the wild-type NT and IBC of $InsP_3R1$, and to the chimeric NT (RyR2A-IBC) is shown in the presence of the indicated concentrations of $InsP_3$. Similar results with adenophostin A are shown in Figure 4b. **c-e**, Specific binding of ^{3}H-$InsP_3$ to chimeric NT with the indicated point mutations within the A-domain of RyR2. Results are means ± s.e.m. from ≥ 3 experiments. Summary data, and their comparison with similar mutations in $InsP_3R1$, are shown in Figure 4c.

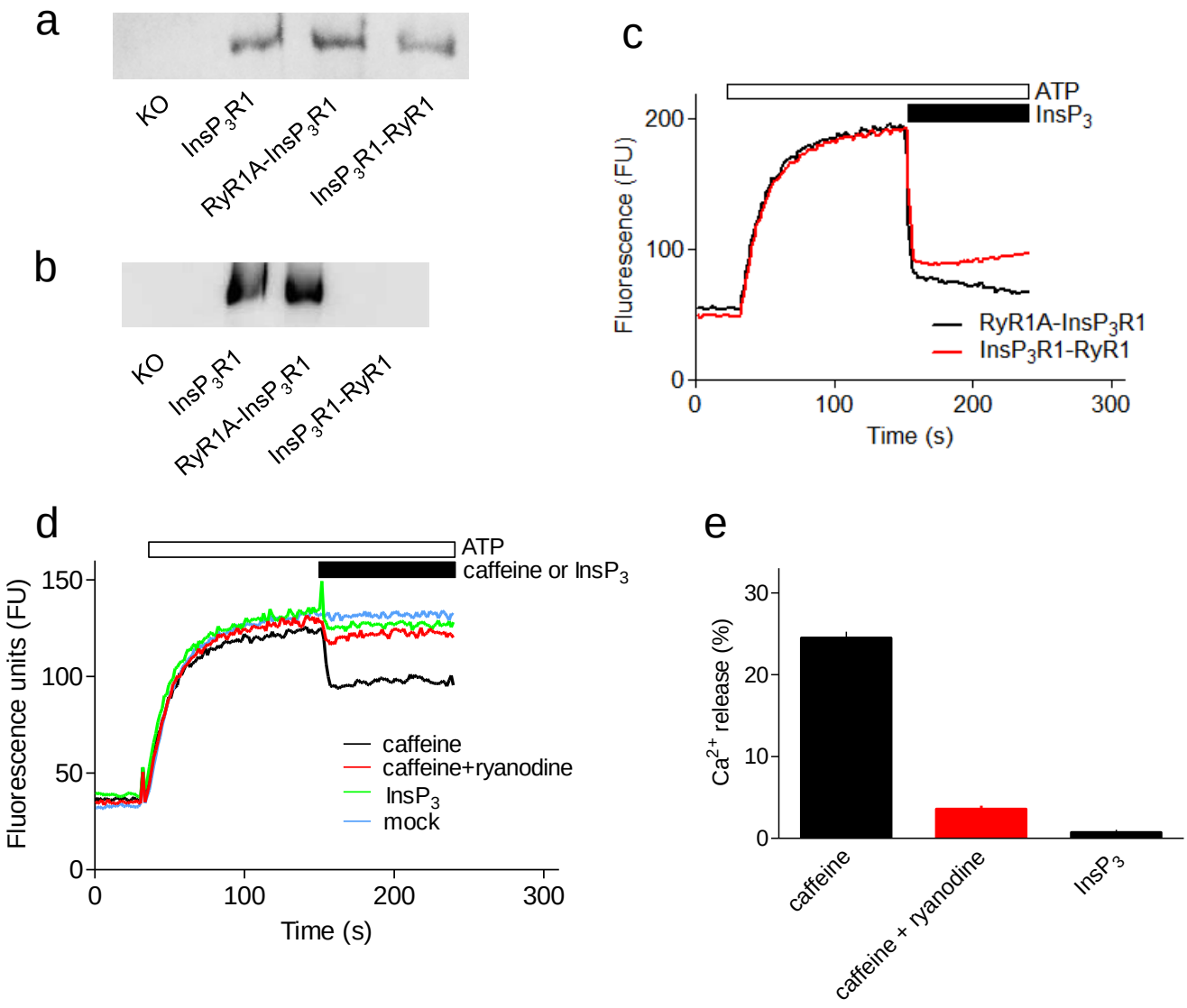

Supplementary Figure 9 | Functional expression of full-length $InsP_3R$, RyR and chimeras in DT40 cells. **a**, **b**, Western blots using anti-peptide antisera that recognize peptide sequences within the IBC (**a**) or C-terminal (**b**) of $InsP_3R1$ show stable expression of the indicated $InsP_3R$ in DT40 cells. Each lane was loaded with protein derived from 3 x 10^7 cells. The blots are typical of 3 similar analyses. Summary of the quantitative analysis of $InsP_3R$ expression is presented in Supplementary Table 7. **c**, Results (typical of at least 4 similar experiments) from functional assays of permeabilized DT40 cells stably expressing RyR1A-$InsP_3R1$ (black) or $InsP_3R$-RyR1 (red). Addition of ATP allowed Ca^{2+} uptake into the ER (detected as an increase in the fluorescence of a luminal Ca^{2+} indicator). When the stores had loaded to steady-state with Ca^{2+} (~2 min), $InsP_3$ (10 µM) was added. **d**, We have not succeeded in establishing DT40 cells stably expressing RyR, but after transient transfection with EGFP-RyR1, 37 ± 2% (n = 3) of cells expressed RyR1. Transient transfection with untagged RyR1 was therefore used to assess the effects of caffeine (10 mM), caffeine with ryanodine (10 µM, added with ATP) or $InsP_3$ (10 µM) on RyR1. The mock-transfected cells were stimulated with caffeine. Results show average results from 4 wells from a single experiment that was repeated 3 times. **e**, Summary data (means ± s.e.m., n = 3) show the percentage of the ATP-dependent Ca^{2+} uptake released by the indicated treatments.

a

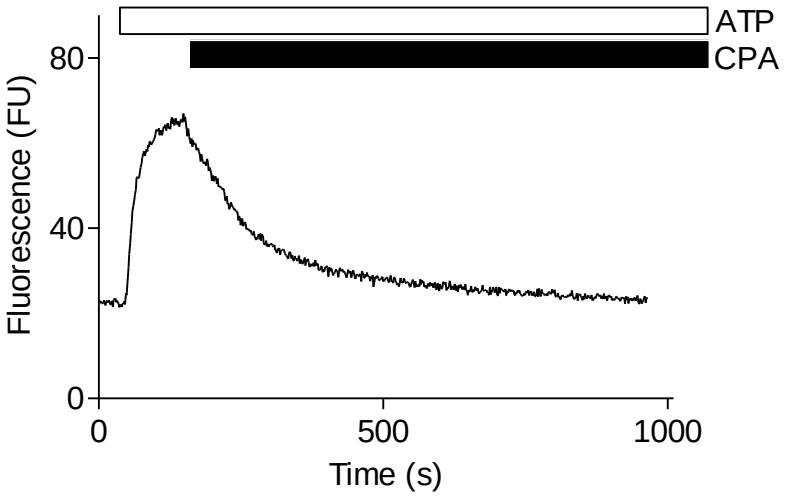

b

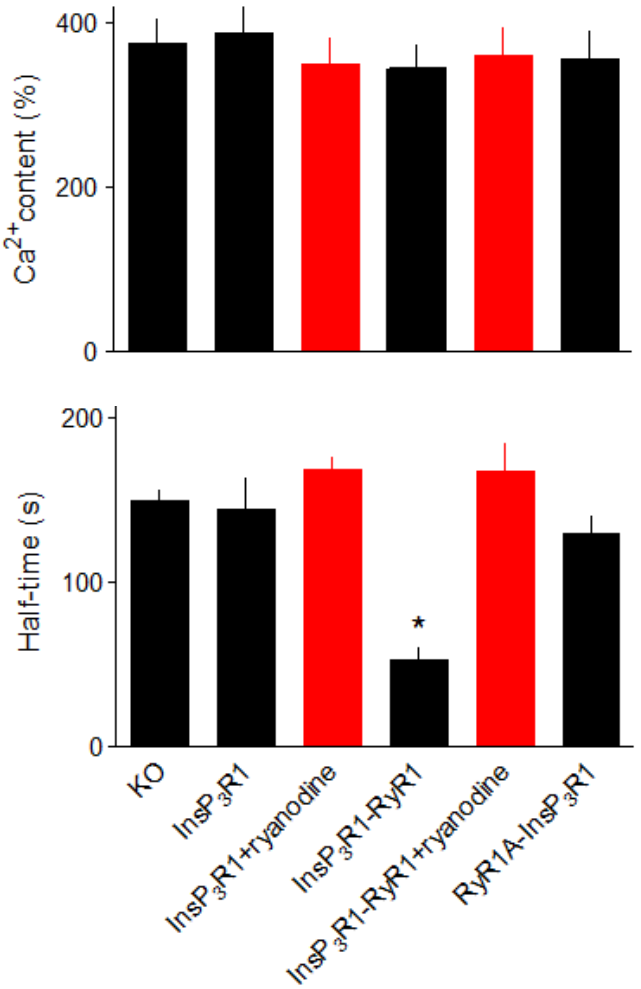

Supplementary Figure 10 | Chimeric $InsP_3R$ have minimal spontaneous activity. a, Typical experiment showing ATP-dependent Ca^{2+} uptake into the intracellular stores of permeabilized DT40-KO cells, followed by addition of cyclopiazonic acid (CPA, 100 μM) to inhibit the ER/SR Ca^{2+}-ATPase (SERCA) from which the half-time ($t_{½}$) for Ca^{2+} release was computed. The Ca^{2+} content of the ER is reported in fluorescence units (FU), which previous work established are linearly related to the free [Ca^{2+}] within the ER[69]. **b**, Summary results (mean ± s.e.m., n = 3) from DT40 cells expressing each of the indicated $InsP_3R$ show the steady-state ATP-dependent Ca^{2+} content of the stores (as % of the fluorescence recorded before addition of ATP) and the $t_{½}$ for Ca^{2+} efflux. **P* < 0.05 relative to DT40-KO cells. Where ryanodine (10 μM) was included, it was added with the ATP.

a

Transmembrane domains

TMD1

```
RyR1     4559  FYTLRFLALFLAFAINFILLFLKVSDSPPGEDDMEGSAAGDLAGAGSGGGSGWGSGAGEEAEGDEDENMVYYFLEEST
InsP3R1  2274  WSSISFNLAVLMNLLVAFFYPFKGVRGGTLEPH----------------------------------------------
```

TMD2

```
RyR1     4637  GYMEPALWCLSLLHTLVAFLCIIGYNCLKVPLVIFKREKELARKLEFDGLYITEQPGDDDVKGQWDRLVLNTPSFPSN
InsP3R1  2307  ----WSGLLWTAMLISLAIVIALPKPHGIRALIASTILRLIFSVGLQPTL----------------------------
```

TMD3

```
RyR1     4715  YWDKFVKRKVLDKHGDIFGRERIAELLGMDLASLEITAHNERKPDPPPGLLTWLMSIDVKYQIWKFGVIFTDNSFLYL
InsP3R1  2353  ------------------------------------------------------------FLLGAFNVCNKII
```

TMD4

```
RyR1     4793  GWYMVMSLLGHYNN----------FFFAA-HLLDIAMGV---KTLRTIL--------------SSVTHNGKQLVMTV
InsP3R1  2366  FLMSFVGNCGTFTRGYRAMVLDVEFLYHLLYLLICAMGLFVHEFFYSLLLFDLVYREETLLNVIKSVTRNGRSIILTA
```

TMD5

```
RyR1     4842  GLLAVVVYLYTVVAFNFFR--------KFYNKS-----------------------------------------EDEDE
InsP3R1  2444  VLALILVYLFSIVGYLFFKDDFILEVDRLPNETAGPETGESLANDFLYSDVCRVETGENCTSPAPKEELLPVEETEQD
```

TMD6

```
RyR1     4872  PDMKCDDMMTCYLFHMYVGVRAGGGIGDEIEDPAGDEYELY-RVVFDITFFFFVIVILLAIIQGLIIDAFGELRDQQE
InsP3R1  2522  KEHTCETLLMCIVTVLSHGLRSGGGVGDVLRKPSKEEPLFAARVIYDLLFFFMVIIIVLNLIFGVIIDTFADLRSEKQ
```

```
RyR1     4949  QVKEDMETKCFICGIGSDYFDTTPHGFETHTLEEHNLANYMFFLMYLINKDETEHTGQESYVWKMYQERCWDFFP---
InsP3R1  2600  KKEEILKTTCFICGLERDKFDNKTVTFEEHIKEEHNMWHYLCFIVLVKVKDSTEYTGPESYVAEMIRERNLDWFPRMR
```

```
RyR1     5024  -----------AGDCFR---------------------KQYEDQLS---------------------------
InsP3R1  2678  AMSLVSSDSEGEQNELRNLQEKLESTMKLVTNLSGQLSELKDQMTEQRKQKQRIGLLGHPPHMNVNPQQPA
```

b

Suppressor and A domains

```
RyR1     1     MGDGGEGEDEVQFLRTDDEVVLQCSATVLKEQLKLCLAAEGFGNRLCFLEPTSNAQNVPP-DLAICCFTLEQSLSVRA
RyR2     1     MADGGEGEDEIQFLRTDDEVVLQCTATIHKEQQKLCLAAEGFGNRLCFLESTSNSKNVPP-DLSICTFVLEQSLLVRA
InsP3R1  1     -----MSDKMSSFLHIGDICSLYAEGSTNG-----FISTLGLVDDRCVVQPEAGDLNNPPKKFRDCLFKLCPMNRYSA
```

```
RyR1     78    LQEML------ANTVEAG------------VESSQGGGHRTLL-----YGHAILLRHAHSRMYLSCLTTSRSMTDKLA
RyR2     78    LQEML------ANTVEKSEGQVDVEKWKFMMKTAQGGGHRTLL-----YGHAILLRHSYSGMYLCCLSTSRSSTDKLA
InsP3R1  69    QKQFWKAAKPGANSTTDAVLLNKLHHAADLEKKQNETENRKLLGTVIQYGNVIQLLHLKSNKYLTVNKRLPALLEKNA
```

```
RyR1     133   FDVGLQEDATGEACWWTMHPASKQRSEGEKVRVGDDLILVSVSSERYLHLS-----TASGELQVDASFMQTLWNMNPI
RyR2     145   FDVGLQEDTTGEACWWTIHPASKQRSEGEKVRVGDDLILVSVSSERYLHLS-----YGNGSLHVDAAFQQT-------
InsP3R1  147   MRVTLDEAGN-EGSWFYIQPFYKLRSIGDSVVIGDKVVLNPVNAGQPLHASSHQLVDNPGCNEVNSVNCNTSWKIVLF
```

```
RyR1     206   CSCCE
RyR2           -----
InsP3R1  224   M----
```

Supplementary Figure 11 | Sequence comparisons of fragments used to generate chimeric $InsP_3R$. a, **b**, Alignments are shown for the fragments that were exchanged to produce chimeras. A variety of experimental and *in silico* analyses[68,37] suggest the presence of six TMDs in both $InsP_3R$ and RyR (**a**). Positions of the predicted TMDs (boxed), the selectivity filter (green shading), and conserved Cys within the C-terminal tail that are essential for gating of $InsP_3R1$[5] (blue) are shown. Sequences within TMD4, the TMD4-5 linker, and all residues from TMD5 onwards were separately aligned (ClustalW 2). Identical residues within these more conserved regions are shown in red. There is no obvious sequence similarity within TMDs1-3 or the intervening loops of RyR and $InsP_3R$. The SD ($InsP_3R1$) and A-domain (RyR1 and RyR2) were aligned using ClustalW 2 (**b**).